1-1-2007

All-dielectric unidirectional dual-grating output coupler

Andrew B. Greenwell
University of Central Florida

Sakoolkan Boonruang
University of Central Florida

M. G. Moharam
University of Central Florida

All-dielectric unidirectional dual-grating output coupler

Andrew B. Greenwell, Sakoolkan Boonruang, and M. G. Moharam

College of Optics and Photonics - CREOL, University of Central Florida
4000 Central Florida Blvd., Orlando, FL 32816-2700
moharam@creol.ucf.edu

Abstract: A novel concept for an all-dielectric unidirectional output double-grating coupler is proposed and rigorously analyzed. In addition to a superstrate side grating, a second grating is placed on the substrate side. The periodicities of the gratings are chosen such that no propagating diffracted orders are present outside the structure in the superstrate region and only a single order is present outside the structure in the substrate region. The concept provides a robust output coupler requiring neither phase-matching between gratings nor any resonances in the structure, and is very tolerant to potential fabrication errors. Up to 96% coupling efficiency from the substrate-side grating is obtained over a wide range of grating properties.

OCIS codes: (050.0050) Diffraction and gratings; (130.0130) Integrated optics.

References

1. T. Tamir, ed., *Integrated Optics* (Springer-Verlag, New York, 1975).
2. V. R. Almeida, R. R. Panepucci, and M. Lipson, "Nanotaper for compact mode conversion," Opt. Lett. **28**, 1302-1304 (2003).
3. T. P. Felici, and D. F. G. Gallagher, "Improved waveguide structures derived from new rapid optimization techniques," in *Physics and Simulation of Optoelectronic Devices XI*, M. Osinski, H. Amano, P. Blood, eds., Proc. SPIE **4986**, 375-385 (2003).
4. B. Luyssaert, P. Bienstman, P. Vandersteegen, P. Dumon, and R. Baets, "Efficient nonadiabatic planar waveguide tapers," J. Lightwave Technol. **23**, 2462-2468 (2005).
5. L. Vaissie, O. V. Smolski, A. Mehta, and E. G. Johnson, "High efficiency surface-emitting laser with subwavelength antireflection structure," IEEE Photon. Technol. Lett. **17**, 732-734 (2005).
6. D. Taillaert, W. Bogaerts, P. Bienstman, T. F. Krauss, P. Van Daele, I. Moerman, S. Verstuyft, K. De Mesel, and R. Baets, "An out-of-plane grating coupler for efficient butt-coupling betweencompact planar waveguides and single-mode fibers," IEEE J. Quantum Electron. **38**, 949-955 (2002).
7. E. G. Johnson, O. V. Smolski, J. K. O'Daniel, A. Mehta, K. Shavitranuruk, P. Srinivasan, and M. G. Moharam, "Micro- and Nano-Optics in Surface Emitting Lasers," in *Nanophotonics* (OSA, Uncasville, CT, USA, 2006).
8. J. K. O'Daniel, O. V. Smolski, M. G. Moharam, and E. G. Johnson, "Integrated wavelength stabilization of in-plane semiconductor lasers by use of a dual-grating reflector," Opt. Lett. **31**, 211-213 (2006).
9. M. G. Moharam, E. B. Grann, D. A. Pommet, and T. K. Gaylord, "Formulation for stable and efficient implementation of the rigorous coupled-wave analysis of binary gratings," J. Opt. Soc. Am. A **12**, 1068-1076 (1995).
10. E. Silberstein, P. Lalanne, J. P. Hugonin, and Q. Cao, "Use of grating theories in integrated optics," J. Opt. Soc. Am. A **18**, 2865-2875 (2001).
11. L. Li, "Formulation and comparison of two recursive matrix algorithms for modeling layered diffraction gratings," J. Opt. Soc. Am. A **16**, 17 (1996).
12. M. G. Moharam, and A. B. Greenwell, "Efficient rigorous calculations of power flow in grating coupled surface-emitting devices," in *Photon Management*, F. Wyrowski; ed., Proc. SPIE **5456**, 57 (2004).
13. P. Dong, and A. G. Kirk, "Compact double-grating coupler between vertically stacked silicon-on-insulator waveguides," Appl. Opt. **44**, 7540-7547 (2005).
14. Q. Cao, P. Lalanne, and J. P. Hugonin, "Stable and efficient Bloch-mode computational method for one-dimensional grating waveguides," J. Opt. Soc. Am. A **19**, 335-338 (2002).
15. P. Lalanne, and J. P. Hugonin, "Bloch-wave engineering for high-Q, small-V microcavities," IEEE J. Quantum Electron., **39**, 1430-1438 (2003).

#76327 - $15.00 USD Received 24 October 2006; revised 27 November 2006; accepted 27 November 2006

1. Introduction

Traditionally, the out coupling of light guided within a planar waveguide has been achieved in one of four manners: end facet couplers, prism couplers, tapered couplers and grating couplers [1]. End facet coupling creates the problems of reflection from a cleaved facet back into the input waveguide mode that can affect the stability of the light source generating the guided wave, the presence of an elliptical spot size created by planar waveguides that normally have vastly different horizontal and vertical dimensions, and the potential for catastrophic end facet damage in high power configurations. Prism coupling eliminates the issues of reflection into an input mode and end facet damage by the use of vertical surface coupling, but the necessity for a prism to have a denser refractive index than the materials comprising the waveguide also precludes the use of prism coupling for high refractive index semiconductor waveguides. Vertically tapered couplers normally consist of an adiabatic variation of the modal index of a waveguide by means of a gradual geometric variation, similar to a prism coupler, but normally results in a large beam divergence. Transversely tapered couplers can be either adiabatic transverse variations [2] or a numerically optimized series of end facet couplings that utilize multilayer resonance effects [3, 4]. In either case, the use of a final end facet coupling retains the same potential for end-facet damage in high power configurations. The use of a surface grating as a means of out coupling from a planar waveguide addresses the weaknesses of both end facet and prism coupling by minimizing reflection into the input waveguide mode and providing a means of surface coupling for any type of material, while also spreading power over a larger surface area and providing numerous degrees of freedom for shaping the output beam.

Grating coupler surface emitting devices tend to have deep grooves in order to interact with the guided mode. This results in diffraction in both a low index superstrate, normally air, and a higher index substrate. Consequently, there is a splitting of the diffracted energy between the substrate and superstrate regions, an example of which can be seen in Fig. 1.

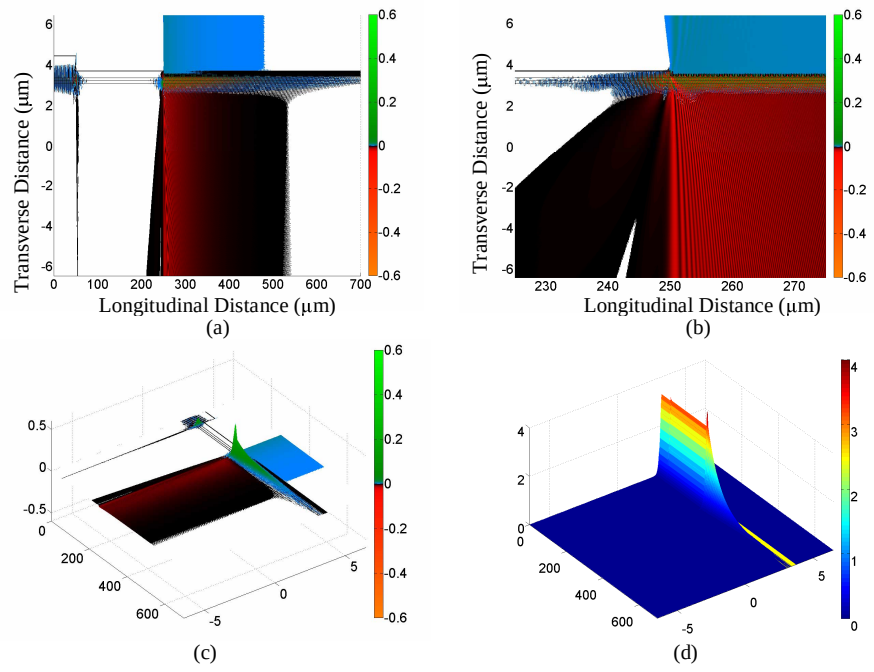

Fig. 1. Power flow in a single surface grating with a 275 nm period, 250 nm depth, and 50% fill factor, which shows the splitting of diffracted energy between a substrate region (70%) and a superstrate region (30%). (a). Transverse power flow over the entire computational window. (b). Transverse power flow near the initial grating interface. (c).-(d). 3D view of transverse and normal power flow showing the power magnitude.

#76327 - $15.00 USD Received 24 October 2006; revised 27 November 2006; accepted 27 November 2006

Attempts to force unidirectional coupling of the diffracted energy have previously involved the addition of either a metallic coating [5] or a thin-film quarter-wave-stack coating to either the grating or the substrate [6]. Metallization of either the grating or the substrate introduces additional absorption and scattering losses which are also problems that should try to be minimized. The addition of a quarter wave stack mirror requires the deposition of additional thin film layers having tight fabrication tolerances, which increases the structure's overall fabrication complexity.

In recent years, the concept of dual-side wafer processing for semiconductor waveguides has been introduced. By integrating a superstrate-side diffraction grating with either a substrate side refractive or diffractive element, numerous applications in spatial and spectral beam control have been introduced [5, 7, 8]. In this work, we present a novel all-dielectric unidirectional grating coupler that avoids the need for any additional material deposition. A model for a unidirectional coupler with a 96% output coupling efficiency is obtained. The dual grating structure is shown to be tolerant to a variety of potential fabrication errors while maintaining a high output power coupling efficiency.

2. Proposed Structure and Device Design Methodology

2.1 Proposed Structure

The device considered consists of a single mode high index waveguide with a superstrate grating that does not produce diffraction in the superstrate air region and diffracts only a single order into the substrate, as well as a substrate side grating that diffracts a single order in the substrate side air region as shown in Fig. 2.

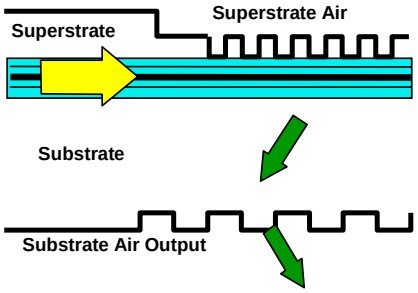

Fig. 2. A simple drawing of the dual grating output coupler device considered in this study, as well as the principal directions of energy flow in the structure.

The periodicity for the superstrate side grating must result in that the guided mode diffraction by the grating produces no propagating diffracted orders in air and only produces a single diffracted order in the substrate region. This is determined from the grating equations:

$$k_{\text{tangential,diffracted}} = k_{\text{tangential,mode}} - pK_{\text{sup}}$$
$$n\sin\theta_{dif} = n_{\text{mode}} - p\frac{\lambda_0}{\Lambda_{\text{sup}}} \quad (1)$$

where λ_0 is light wavelength, Λ_{sup} is the periodicity of the superstrate grating, p is the diffracted order, and n is the average refractive index of the region where the diffraction occurs. In order to restrict the propagation of diffracted orders in air, the upper bound on the superstrate periodicity is as follows:

$$\Lambda_{\text{sup}} < \lambda_0/(n_{\text{mode}}+1) \quad (2)$$

To ensure the propagation of at least a single diffracted order in the substrate region (n_{sub}), the lower bound on the superstrate periodicity obeys the following inequality:

$$\Lambda_{\text{sup}} > \lambda_0/(n_{\text{mode}}+n_{sub}) \quad (3)$$

#76327 - $15.00 USD Received 24 October 2006; revised 27 November 2006; accepted 27 November 2006

For the grating on the substrate side, the grating equation is as follows:

$$\sin\theta_{dif,out} = \sin\theta_{air} = \left(n_{\text{mode}} + \frac{\lambda_0}{\Lambda_{\text{sup}}} \right) - p\frac{\lambda_0}{\Lambda_{\text{sub}}} \tag{4}$$

To ensure that the substrate grating will produce only a single diffracted order in air, its periodicity is determined by the following inequalities:

$$\lambda_0 / \left(n_{\text{mod}e} - \sin\theta_{air} + \lambda_0 / \Lambda_{\text{sup}} \right) < \Lambda_{sub} < 2\lambda_0 / \left(n_{\text{mode}} - \sin\theta_{air} + \lambda_0 / \Lambda_{\text{sup}} \right) \tag{5}$$

To investigate the properties and behavior of the proposed dual grating structure, the properties of each individual grating are rigorously studied by means of the Rigorous Coupled Wave Analysis (RCWA), using both its original form for infinite transverse gratings [9] and its application to finite-sized integrated optical structures [10-12]. Finally, the integration of both gratings in a single device is studied using this same finite waveguide eigenmode expansion method. A similar approach to modeling an integrated dual grating directional coupler using a different eigenmode expansion technique has been used previously as well [13].

2.2 Single Mode Waveguide

The waveguide under consideration consists of a multi-quantum well $Al_xGa_{1-x}As$ region of tens of nanometer thickness (n ~ 3.6) surrounded by equivalent graded index Al_xGa_{1-x} regions of roughly 200nm in thickness (3.24 < n < 3.5) on top of a GaAs substrate (n = 3.24). A superstrate GaAs cladding layer is added on top of the graded index layers. Using a modal solver with incorporated Perfectly Matched Layer (PML) boundary conditions, the modal index of this TE single mode waveguide considered at a 980 nm wavelength is determined to be 3.355. Figure 3 shows the longitudinal component of the time-averaged Poynting vector associated with this waveguide mode.

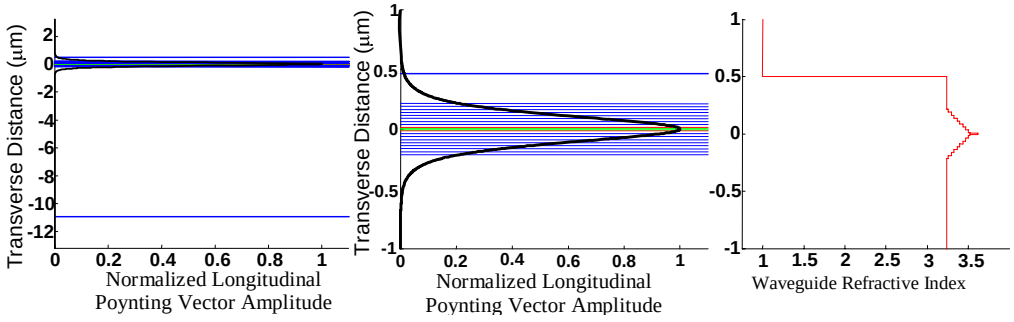

Fig. 3. The normalized longitudinal Poynting vector component and refractive index distribution of the single mode waveguide showing both location and size of the graded index section relative to the substrate and the power distribution within the graded index section.

2.3 Bounds on grating periodicities

The modal index of the single mode waveguide is then used to determine the range of periodicities allowing for unidirectional output coupling from the substrate side of the device. For a modal index, n_{mode} = 3.355, the upper limit of the superstrate side grating periodicity is 225 nm (which ensures no diffraction in air). For a substrate region average index, n_{sub} = 3.24, the lower limit of the superstrate-side grating periodicity is 148 nm (which ensures the presence of diffraction into the substrate). As shown in (5), the range on the substrate grating period depends upon the choice for the superstrate grating period, which determines the incident and exit angles for the substrate grating.

#76327 - $15.00 USD Received 24 October 2006; revised 27 November 2006; accepted 27 November 2006

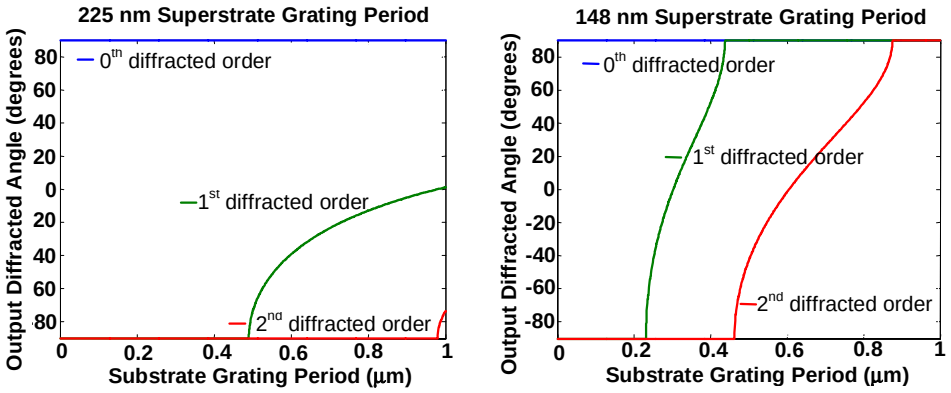

Fig. 4. The output diffracted angle in air vs. the substrate grating period, for substrate index of $n_{sub} = 3.24$, and a superstrate grating period of (a) 225 nm. and (b) 148 nm.

As shown in Fig. 4(a), for a superstrate grating period of 225 nm, the substrate grating period can take a value of anywhere from 490 nm (where the 1st order begins propagating) to 979 nm (where the 2nd order begins propagating). Similarly Figure 4(b) shows that for a superstrate grating period of 148 nm, the substrate grating period can range from 231 nm to 437 nm. With a choice of superstrate grating period between 148 nm and 225 nm, the potential periodicity range for the substrate grating moves accordingly, but as shorter periodicities produce larger diffracted angles into the substrate, it is desirable to choose a period at the longer end of this range.

2.4 Determination of proper individual grating strengths

Once the ranges of potential superstrate and substrate grating periodicities are known, the gratings can then be evaluated on the basis of their diffractive strengths. For the superstrate and substrate gratings, properties such as the grating periodicity, depth, fill factor, and profile all contribute to how power is diffracted away from the input waveguide mode and out of the device substrate.

Since the superstrate grating affects the coupling loss from the input mode most significantly, its properties are investigated first. To analyze the superstrate grating in isolation, PML boundary conditions are placed adjacent to the superstrate air region and the GaAs substrate. A virtually semi-infinite grating coupler (length ~1 m) is used to ensure that all the energy is coupled out and no reflection occurs from a possibly mismatched output half-space waveguide. However, coupled energy was only collected over a finite length (~700 μm) which is found to be sufficient, in most cases, to collect all power that is scattered in the transverse direction by the structure as shown in Fig. 5.

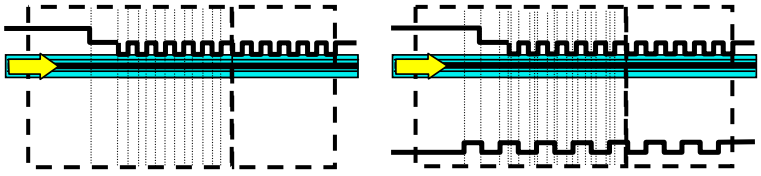

Fig. 5. A sketch showing the computational and power collection windows for both a single surface grating with an "infinite" substrate and a dual grating coupler. Dotted lines represent interfaces used to define layer scattering matrices.

The selection of grating period, thickness, and fill factor for the superstrate grating involves a trade off between the coupling length of the complex grating mode, the modal mismatch between the input waveguide mode and the leaky waveguide-grating mode, and the reasonable ability to fabricate the chosen grating geometry.

#76327 - $15.00 USD Received 24 October 2006; revised 27 November 2006; accepted 27 November 2006

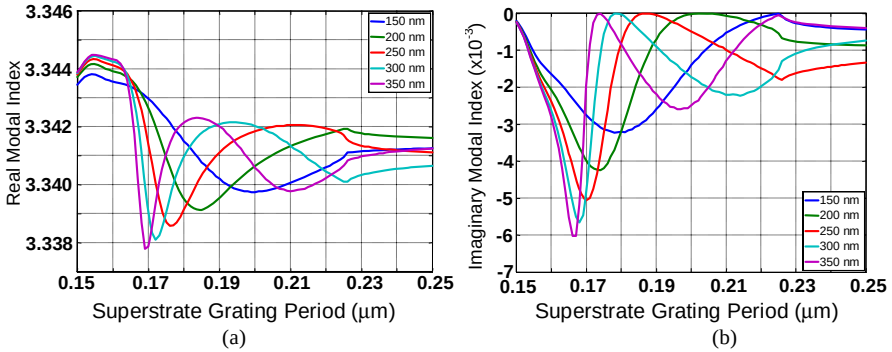

Fig. 6. (a). Real part and (b). imaginary part of the Bloch mode index of the fundamental mode in the superstrate grating vs. superstrate grating period for various grating thicknesses.

Figures 6(a) and 6(b) show the real and imaginary Bloch mode index values vs. period associated with the superstrate grating for various grating thicknesses having a 50% fill factor calculated using the generalized eigenvalue approach described in Cao et. al [14]. While all values within the previously defined superstrate periodicity range will couple nearly all of the input power into the substrate, the variation in modal losses, seen in Fig. 6(b), show that coupling length can vary significantly with grating period and grating depth. A grating period of 220 nm with a grating depth of 250 nm is chosen due to it having a relatively shallow diffraction angle in the substrate (~20º), a significant modal loss for our chosen 50% fill factor, a negligible reflection, and a reasonable depth from a fabrication point of view. Consequently, these parameters are utilized in the remainder of this work. Figures 7(a) through 7(d) show views of the transverse and normal components of the Poynting vector at a 220 nm period, with a 250 nm grating depth and 50% fill factor, which produce a 99.9% coupling efficiency into the substrate.

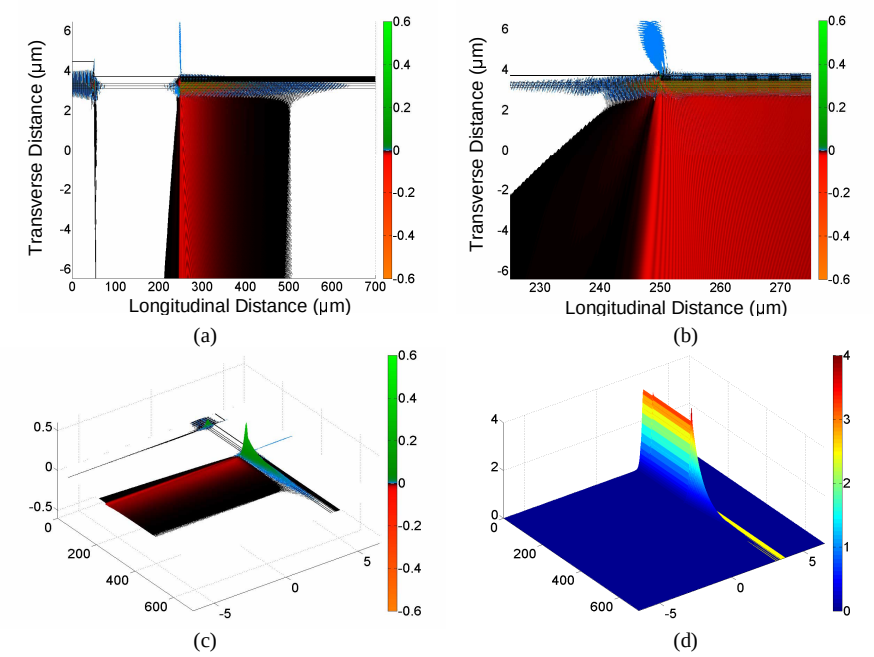

Fig. 7. Power flow in a single surface grating (a) Transverse power flow over the length of the coupler (b) Transverse power flow near the initial grating interface. (c)-(d) 3D view of transverse and normal power flow showing the power magnitude.

#76327 - $15.00 USD Received 24 October 2006; revised 27 November 2006; accepted 27 November 2006

Having analyzed properties for the superstrate grating, we then investigate the substrate grating properties. Using the infinitely periodic, grating form of RCWA, diffraction into the 1st diffracted order in air is calculated for the following set of parameters: a high index input half-space is assigned the refractive index of the GaAs substrate (n = 3.24), a low index output half-space is assigned that of air (n = 1), and the incident angle is assigned as the previously determined superstrate grating diffraction angle into the substrate (~20º). In performing a full parameter scan of the 3 dimensional space of grating period (400 nm to 700 nm), grating depth (25 nm to 525 nm), and fill factor (0 to 1). For the grating under consideration, it is found that a fill factor of 30% produced the highest diffraction efficiency over a wide range of grating periods and depths. The 2D contour plot of 1st order diffraction efficiency vs. grating depth and grating period at a fill factor of 30% is shown in Fig. 8. The diffraction efficiency is calculated to be above 85% within relative a wide range (570-595 nm for the grating period and 250-270 nm for the grating depth). Any grating period and grating depth within these ranges will produce nearly the maximum efficiency.

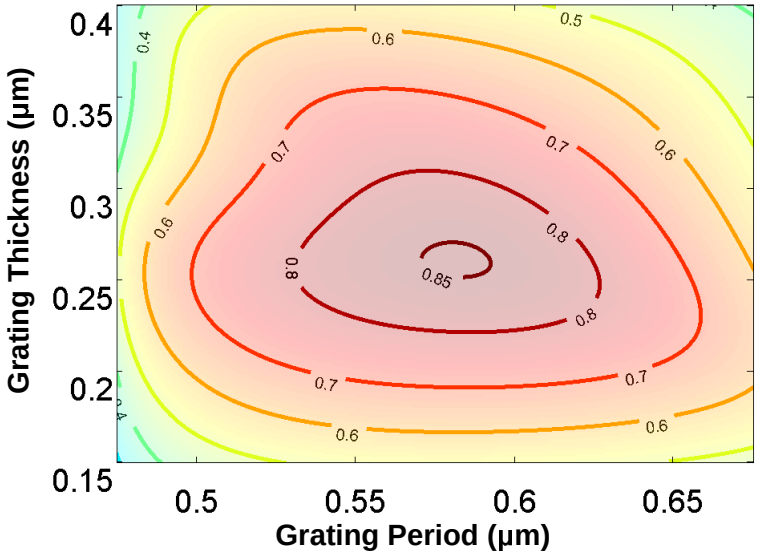

Fig. 8. Contour plot showing the effects of varying grating period and grating depth on the 1st order Transmission efficiency for an infinite binary grating with an input refractive index, n_{input} = 3.24, an output refractive index, n_{output} = 1, a grating tooth refractive index of n_{ridge} = 3.24, a grating groove refractive index, n_{groove} = 1, an input angle, θ_{input} = -19.83º, and a grating fill factor of 30%.

However, to reduce the computational effort it is important for the ratio between the periodicities of the superstrate side and substrate side gratings to have a ratio of two small integers. This reduces the length of the unit cell, as well as the number of layers needed to represent that unit cell. For example a substrate grating period of 582 nm (peak of the range) would result in a grating period ratio of $\Lambda_{superstrate}/\Lambda_{substrate}$ = 110/291 and over 800 distinct layers within the unit cell with a length of just over 64 microns. However, by choosing a grating period integer ratio of 3/8, resulting in a substrate grating period of 586 2/3 nm, the 1st order diffraction efficiency remains above 85%, but the length of the longitudinal unit cell (1.76 μm) and the number of distinct layers (23 layers) within the unit cell are both significantly reduced. A more detailed discussion of the layer slicing necessary for modeling double grating structures in eigenmode expansion techniques can be found in Dong et. al [13].

#76327 - $15.00 USD Received 24 October 2006; revised 27 November 2006; accepted 27 November 2006

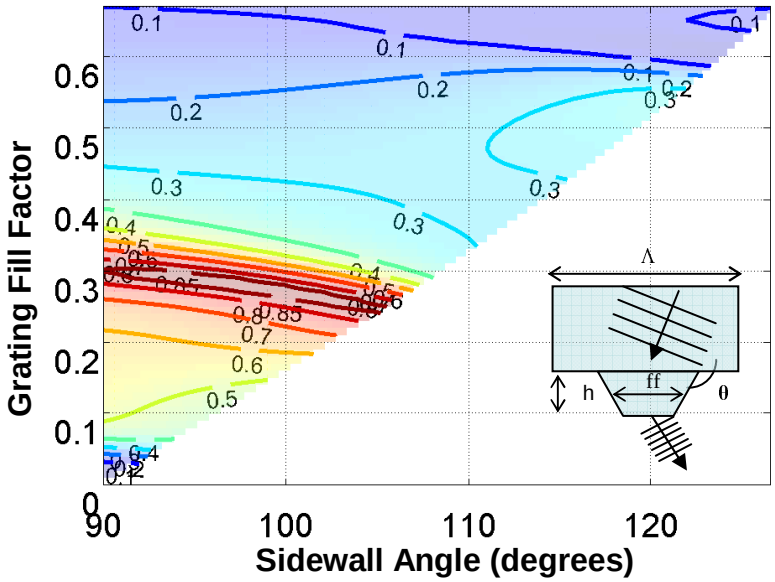

Fig. 9. Contour plot showing the effects of varying the half-height grating fill factor and grating tooth sidewall angle on the 1st order Transmission efficiency for an infinite binary grating with an input refractive index, n_{input} = 3.24, an output refractive index, n_{output} = 1, a grating tooth refractive index of n_{ridge} = 3.24, a grating groove refractive index, n_{groove} = 1, an input angle, θ_{input} = -19.83º, a grating period of 586.66 nm, and a grating depth of 260 nm. Sloped sidewalls are approximated by an 8 level staircase profile. White background regions with a fill factor less than 67% represent gratings with triangular teeth which were not considered.

In Fig. 9, we investigate the effect of the substrate grating profile by determining the 1st order diffraction efficiency of an infinitely periodic substrate grating as a function of the half height fill factor vs. outer sidewall angle for a grating depth of 260 nm. The tapered sidewall angle is approximated by an 8 level staircase profile. Angles that are greater than 90º represent a sloped grating tooth sidewall. Outside of the colored contour plot, the white background indicates grating tooth parameters that will produce a triangular shaped grating tooth and are not considered here. A slightly tapered sidewall angle of 92º at a fill factor of 30% is calculated to have the best diffraction efficiency performance at nearly 86%, but as can be seen in Fig. 9; in the neighborhood of a 25-30% fill factor there is a considerable amount of variation possible in the sidewall angle that maintains greater than 80% transmission efficiency.

2.5 Full Dual Grating Coupler Model

Building on the knowledge gained from investigating the superstrate and substrate grating properties, the performance of the full dual grating coupler device is then explored. For this dual grating structure, the two gratings are separated by a substrate of multiple wavelength thickness. In a real device this substrate is likely to be 100-500 μm in thickness, but to keep practical limits on the required amount of computation time we limited the size to about 10-20 μm such that the utilized number of spatial harmonics will maintain convergence in the eigenvalue problems. The superstrate and substrate gratings are then surrounded by air regions that are then adjacent to PML boundary layers. In order to collect all of the downward diffracted energy from the initial waveguide/superstrate grating interface, the length of the substrate grating is extended from the longitudinal location of the waveguide/superstrate grating interface toward the input interface by an arbitrary length of 150 μm. While this choice of length is more than enough to collect all of the scattered light for a substrate thickness of roughly 10 μm, for a realistic substrate of a few hundred microns a substrate grating extension of this length scale will be critical to collecting all of the scattered

#76327 - $15.00 USD Received 24 October 2006; revised 27 November 2006; accepted 27 November 2006

light. This length choice depends upon the substrate thickness and the angle of diffraction in the substrate. For the structure having simple binary superstrate and substrate gratings, the effect of grating separation on the model is initially tested. As can be seen in Fig. 10(a), by changing the thickness of the substrate, relatively narrow resonances are produced, but by examining Fig. 10(b) representing the reflection into the input interface, as well as the reflection coefficients of all individual modes in the input half-space, these resonances can be attributed to coupling into higher order super-modes of the overall device.

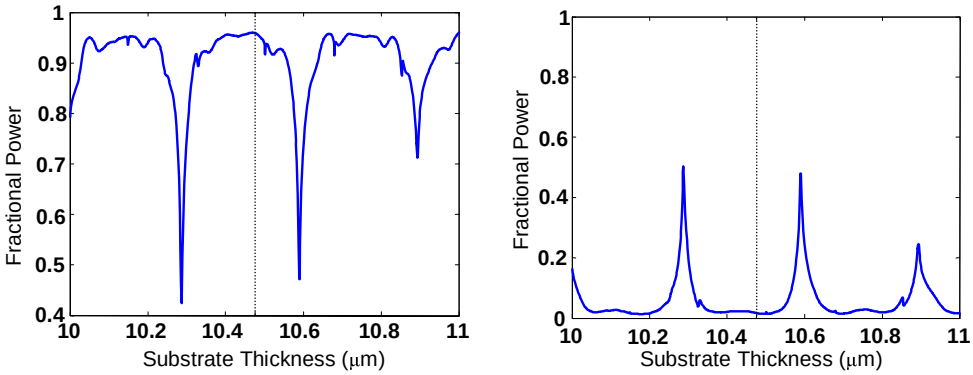

(a) (b)

Fig. 10. (a). Relationship between substrate thickness/grating separation and fractional substrate output coupling. Resonances indicate coupling to higher order super-modes of the entire waveguide stack. (b). Sum of the reflection into all individual modes at the computational window's input interface.

Given that a real device structure will have a slight amount of surface roughness and thickness variation over surface of the wafer; these resonances are most likely just an artifact of the model's "perfect geometry". To avoid this higher order mode coupling, a substrate thickness is chosen, as shown by the dotted line in Fig. 10(a), in a relatively flat region between super-mode coupling resonances.

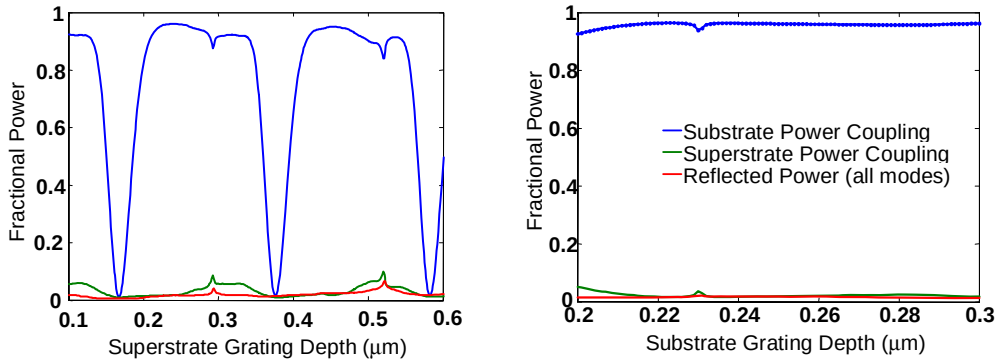

Fig. 11. Substrate output power coupling vs. (a) the superstrate grating thickness and (b) the substrate grating thickness.

Figures 11(a) and 11(b) show the effects that varying superstrate grating thickness and substrate grating thickness in a dual grating structure have on substrate output power coupling efficiency. The narrow resonances in Fig. 11(a) and Fig. 11(b) correspond to super-mode type resonances discussed earlier, while the broader resonances in Fig. 11(a) correspond to increased coupling lengths (decreased modal leakage rates) that cause most of the energy to be guided beyond the 700 μm longitudinal window length.

#76327 - $15.00 USD Received 24 October 2006; revised 27 November 2006; accepted 27 November 2006

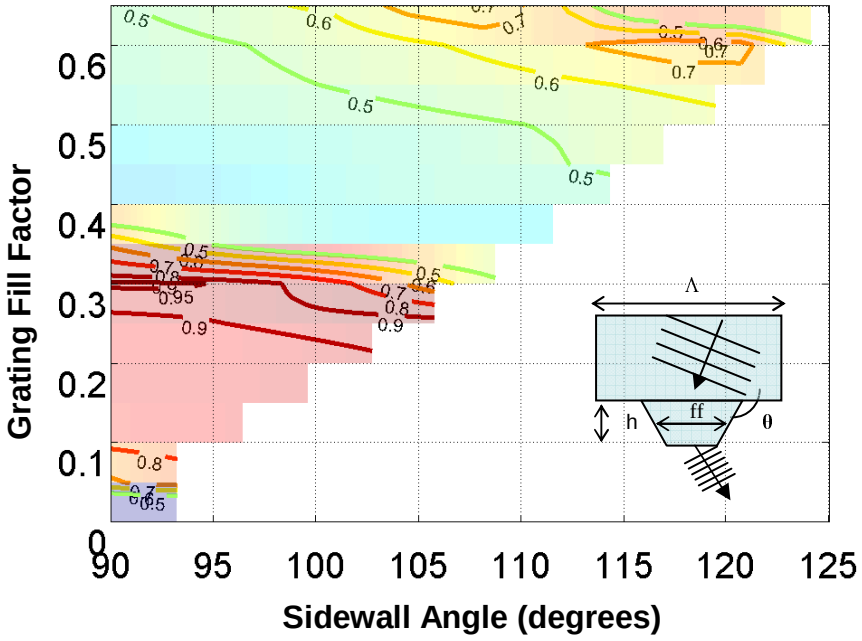

Fig. 12. Map showing the effects of varying the half-height grating fill factor and grating tooth sidewall angle on the substrate output power coupling for the dual grating coupler. As in Fig. 9, the white background regions with a fill factor less than 67% represent gratings with triangular teeth which were not considered.

Figure 12 shows the effects on substrate output power coupling for varying the substrate grating's half-height fill factor and outer side-wall angle. As in the infinite grating model, the peak substrate power coupling efficiency, which in this case is close to 96%, occur near a fill factor of 30% and had a slightly sloped sidewall angle of 92º. As can be seen in Fig. 12, there is a channel in the vicinity of a 25-30% fill factor, where the substrate power coupling efficiency remains above 90% from a sidewall angle of 90º to just over 105º. Both Fig. 11 and Fig. 12 show that for the initial grating parameters determined in the previous section, a robust and tolerant output grating coupler having an output coupling efficiency around 96% can be achieved. As is the case with varying the grating period ratios, to perform sloped side-wall calculations for the dual grating device, stair-casing of the gratings increases the number of layer interfaces, distinct eigenvalue problems, and scattering matrices required within a longitudinal unit cell.

Figure 13 shows the normal and transverse Poynting vector components for a dual grating coupler having a superstrate grating period, fill factor, and thickness of 220 nm, 50%, and 250 nm respectively, as well as a substrate grating period, fill factor and thickness of 586.66 nm, 30% and 260 nm respectively. Within the 700 μm longitudinal power collection window, the substrate power coupling efficiency is nearly 96%, with just over 2% coupled from the superstrate side of the device (primarily at the initial interface of the superstrate grating), and just under 2% coupled into all modes of the input interface. The substrate coupling efficiency can likely be improved upon even further by using a tapered transitional superstrate grating period similar to the approach used in Lalanne et. al [15]. Chirping the superstrate grating fill factor [5], depth, or period will also provide for the ability to shape the spatial distribution of output power, but will admittedly make the computational design process much more costly in time and memory requirements

#76327 - $15.00 USD Received 24 October 2006; revised 27 November 2006; accepted 27 November 2006

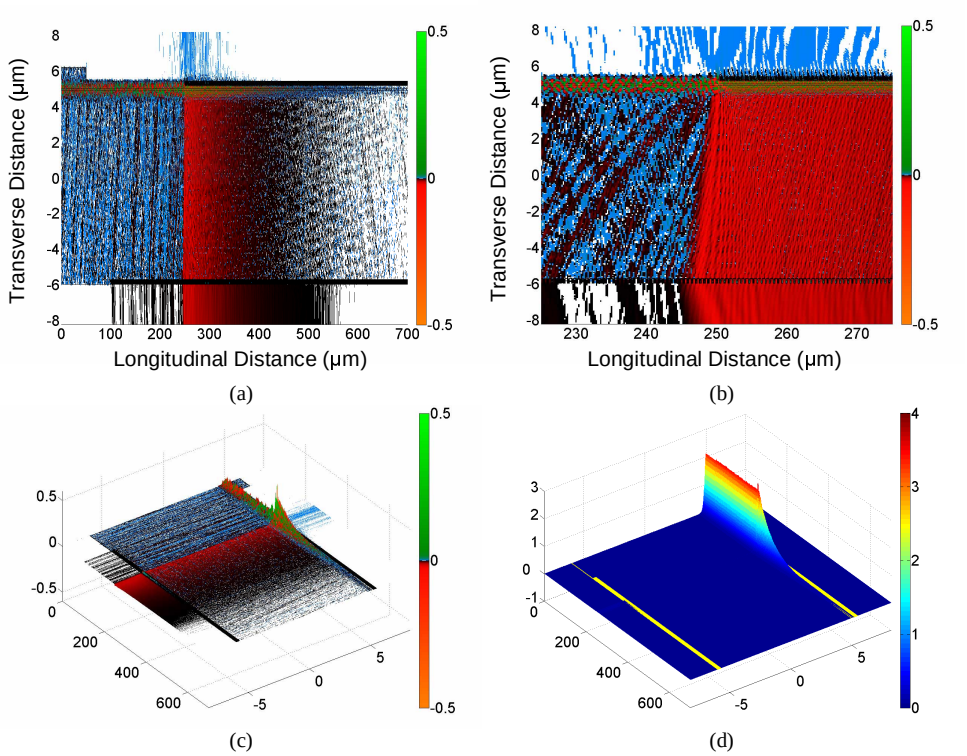

Fig. 13. Power flow in a dual grating coupler with a superstrate grating having a 220 nm period, 250 nm depth, and 50% fill factor, and a substrate grating having a 586.67 nm period, a 260 nm depth, and a 30% fill factor, which show the splitting of diffracted energy between the substrate region (96%) and superstrate region (~2%). (a) Transverse power flow over the entire computational window. (b) Transverse power flow near the initial superstrate grating interface. (c)-(d) 3D view of transverse and normal power flow showing the power magnitude.

Figure 14(a) shows the near-field transverse Poynting vector component at 2 μm from the substrate grating surface and Fig. 14(b) shows the angular spectrum of this Transverse Poynting vector component calculated using a discrete Fourier transform performed on our non-uniformly spaced longitudinal sampling window. As can be seen in this angular spectrum the vast majority of the light coupled from the device is located in a very narrow angular range around a diffraction angle of 34º.

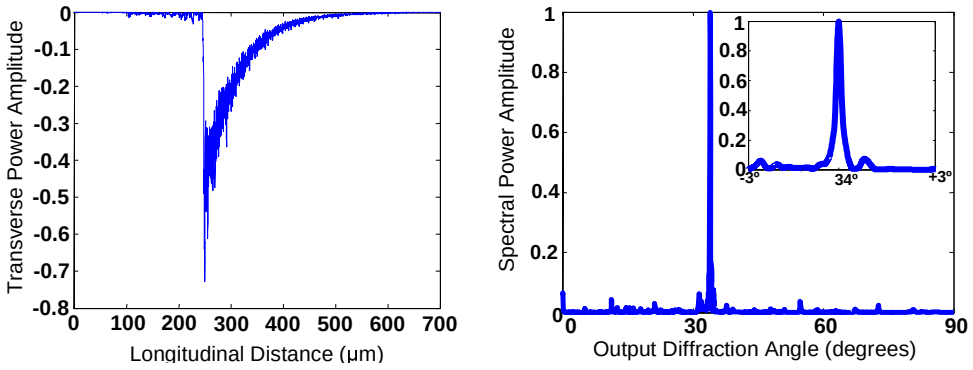

Fig. 14. (a). Transverse power flow in air at 2 μm from the surface of the substrate grating. (b) Angular spectrum of the transverse power in air, and an inset showing the shape of the angular spectrum at ± 3º of its maximum value.

#76327 - $15.00 USD Received 24 October 2006; revised 27 November 2006; accepted 27 November 2006

Figure 15(a) shows this Transverse Poynting vector component propagated through 100 μm of air by performing an inverse discrete Fourier transform. Figure 15(b) shows this same transverse Poynting vector component spatially filtered at ±3º around the peak 34º angular spectrum component, which clearly shows how energy can be concentrated in a particularly narrow angular range and whose spectral profile can be maintained over a long propagation distance.

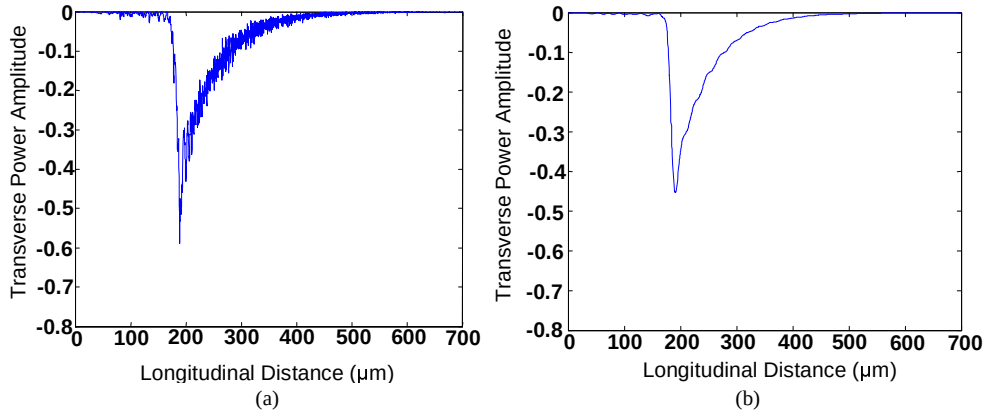

Fig. 15. (a). Transverse power flow in air at 100 μm from the surface of the substrate grating, calculated by propagating the angular spectrum using an Inverse Discrete Fourier Transform. (b) Transverse power flow in air at 100 μm from the surface of the substrate grating spatially filtered at ± 3º of the maximum angular spectrum component.

3. Conclusion

By rigorously modeling, both separately and together, the waveguide and two gratings contained in a dual grating device, a novel all-dielectric unidirectional output grating coupler was designed. The all-dielectric dual grating coupler is robust in that it does not depend on any type of resonance or any type of phase matching between the two gratings and is also tolerant to potential variations in numerous grating parameters. The device eliminates the need for any additional material deposition post-etching and fits neatly within the recently developed framework of dual sided wafer processing.

Acknowledgments

The authors would like to thank Dr. Eric Johnson for fruitful discussions in developing this work. Author Andrew Greenwell would also like to thank everyone at Interactive Supercomputing Corporation (http://www.interactivesupercomputing.com) for providing access to one of their servers as well as access and support for their Star-P software, which was utilized for some of the computations performed in this work.

#76327 - $15.00 USD Received 24 October 2006; revised 27 November 2006; accepted 27 November 2006